Performance of Photon-Counting Detector CT for Electron Density and Effective Atomic Number Maps

Maryam Sadeghian, MS[1]; Du Zhang, PhD[1]; Elisabeth R Shanblatt, PhD[2]; Patrick Wohlfahrt, PhD[3]; Markus Juergens, PhD[3]; Yanle Hu, PhD[4]; Cynthia H. McCollough, PhD[1]; Shuai Leng, PhD[1]

[1]Department of Radiology, Mayo Clinic, Rochester, MN, USA; [2]Siemens Medical Solutions, 40 Liberty Boulevard, Malvern, PA, USA; [3]Siemens Healthineers, Varian, Cancer Therapy Imaging, Forchheim, Germany; [4]Department of Radiation Oncology, Mayo Clinic, Phoenix, AZ, USA

INTRODUCTION

Multi-energy CT enables extraction of relative electron density (RED) and effective atomic number (Z_{eff})[1], which are essential for radiotherapy treatment planning and dose calculation.[1,2] Dual-energy CT (DECT) using energy-integrating detectors (EID) derives spectral information from dual-kV acquisitions, rapid kV switching, or other methods.[3,4] In contrast, photon-counting detector CT (PCD-CT) directly counts individual photons and bins them by energy in a single acquisition, providing improved spatial resolution, reduced electronic noise, and potentially higher quantitative accuracy.[5,6] However, the quantitative performance of PCD-CT across clinically relevant patient sizes and tube potentials remains incompletely characterized. This study evaluates PCD-CT against dual-energy EID-CT for RED and Z_{eff} quantification across phantom sizes.

METHODS

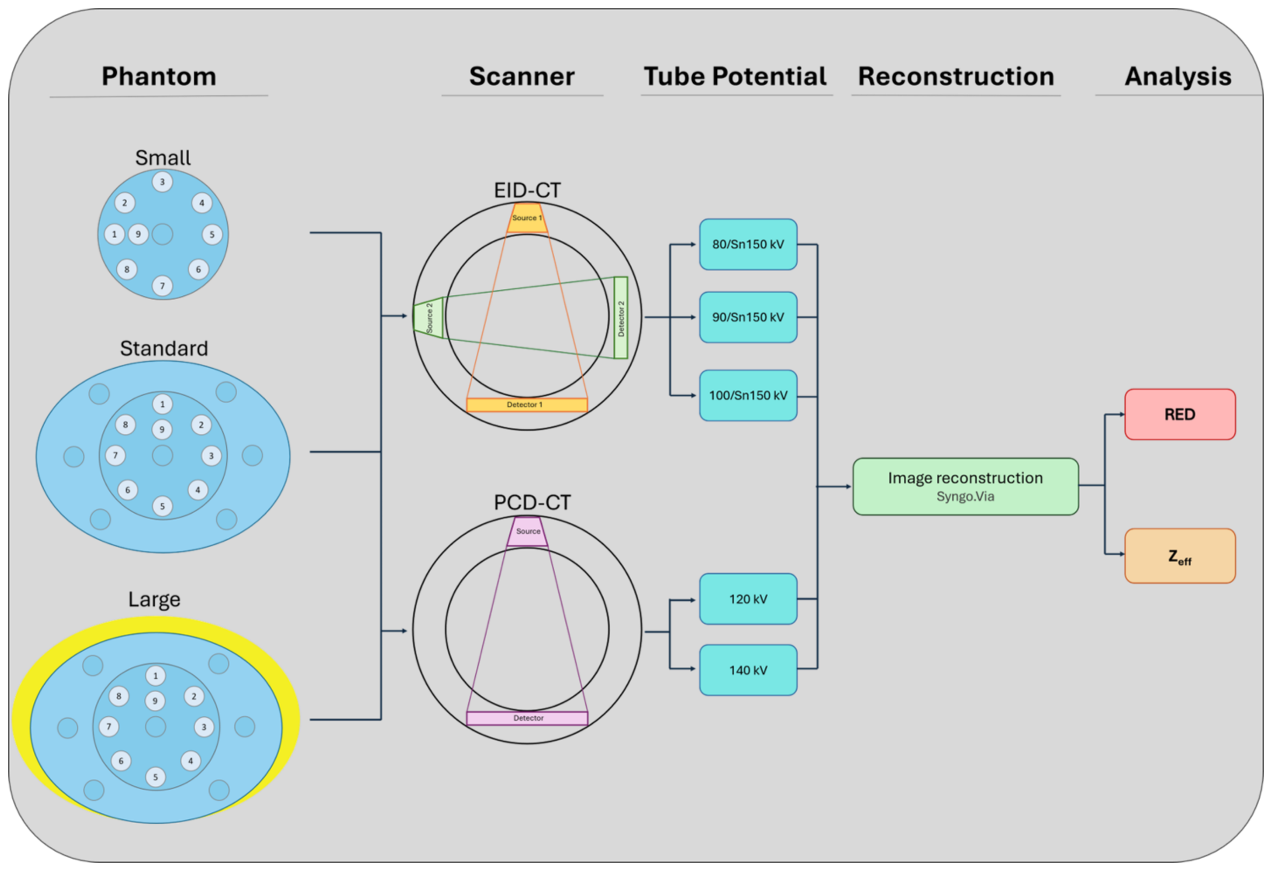

Figure 1. Workflow of the study using Gammex phantoms (20, 40, 50 cm). Nine tissue-equivalent inserts: (1) liver, (2) cortical bone, (3) solid water, (4) $CaCO_3$ (30%), (5) brain, (6) breast (50/50), (7) inner bone, (8) blood (100 HU), (9) adipose. Scans performed on PCD-CT (120, 140 kV) and EID-CT (80/Sn150, 90/Sn150, 100/Sn150 kV). Relative electron density (RED) and Z_{eff} maps generated.

A Gammex Multi-Energy CT phantom was scanned in three configurations representing different body sizes: 20 cm (pediatric), 40 cm (standard adult), and 50 cm (large body habitus).

Each configuration contained 9 tissue-equivalent inserts with known physical properties: adipose, breast (50/50), brain, liver, blood (100 HU), inner bone, cortical bone, $CaCO_3$ (30%), and solid water.

Reference RED values were provided by the manufacturer. Zeff values were derived from elemental composition using established physical modeling.

Imaging was performed on:

- PCD-CT (NAEOTOM Alpha): 120 and 140 kV
- EID-CT (SOMATOM Force): 80/Sn150, 90/Sn150, 100/Sn150 kV

All scans were performed with automatic exposure control (CAREkeV, CAREDose4D). $CTDI_{vol}$ was matched between systems for each phantom size.

Reconstruction was performed with a quantitative kernel (Qr40) and 2 mm slice thickness. RED and Z_{eff} maps were generated by commercial software (Syngo.via).

Circular ROIs were placed in each insert to extract mean values and standard deviation (noise).

Mean absolute error (MAE) and percentage error were assessed across scanners, tube potentials, and phantom sizes.

RESULTS

Relative Electron Density (RED) Accuracy

PCD-CT showed improved accuracy at higher tube potential:

- PCD-CT 140 kV: MAE 0.0037–0.0052 (0.33–0.45%)
- PCD-CT 120 kV: MAE 0.014–0.017 (1.23–1.51%)
- EID-CT (all DE modes): MAE 0.0046–0.0115 (0.39–1.01%)

Performance advantage of PCD-CT was most pronounced at 140 kV and remained consistent across all phantom sizes.

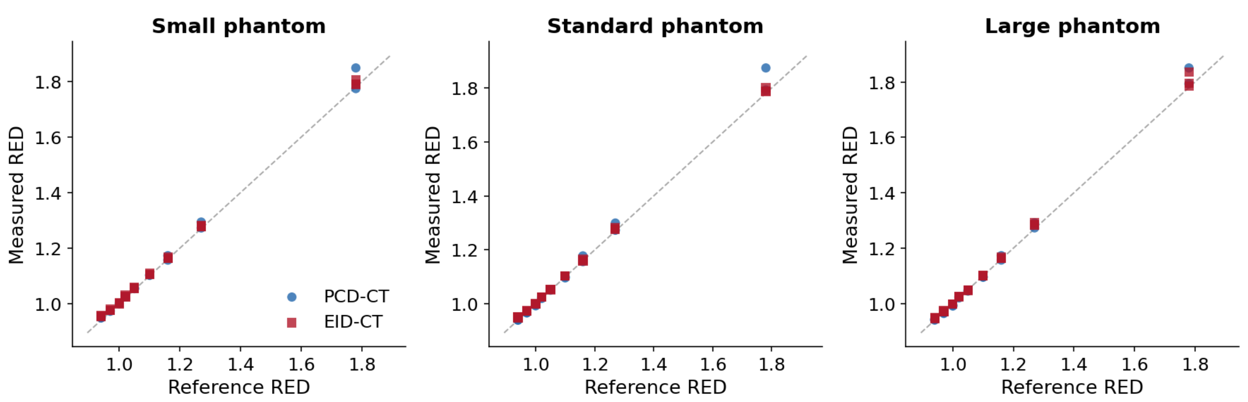

Figure 2. Measured versus reference RED for PCD-CT (blue) and EID (red) for small, standard, and large phantoms. Data from all tube potentials are pooled within each scanner group. Dashed line represents identity line.

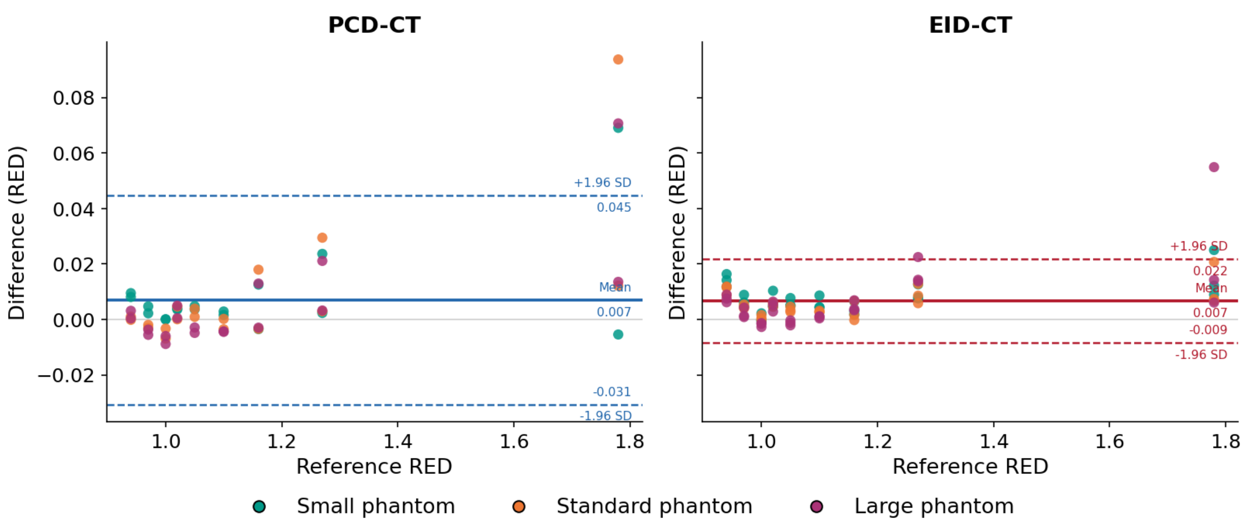

Figure 3. Bland-Altman plots for RED show the difference between measured and reference RED plotted against reference RED from PCD-CT (left) and EID-CT (right). Each point represents one insert at one tube potential. All tube potentials pooled within each scanner.

Effective Atomic Number (Z_{eff})

Z_{eff} values were comparable between CT systems

- MAE: 0.2–0.4 (~2.67–5.68%)
- No significant dependence on phantom size or tube potential
- Similar performance across PCD-CT and EID-CT

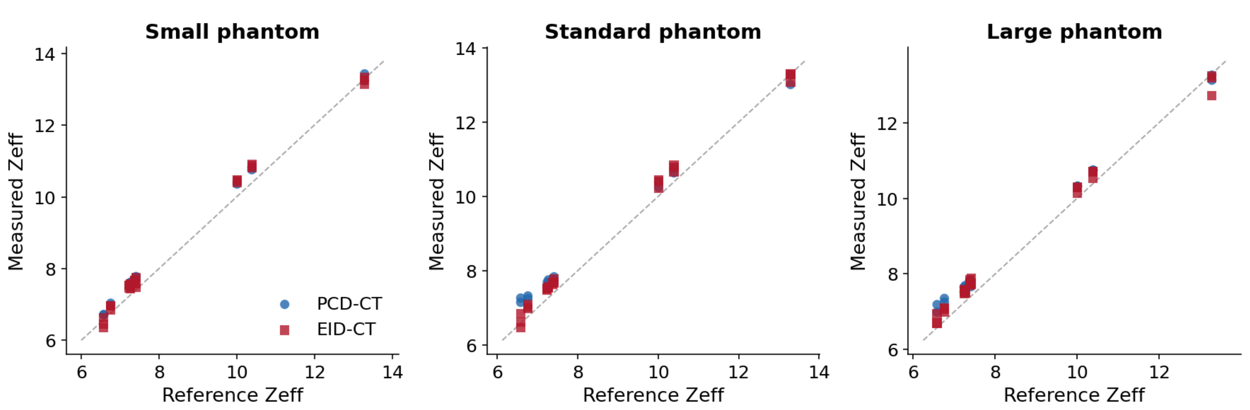

Figure 4. Measured versus reference Z_{eff} for PCD-CT (blue) and EID (red) across small, standard, and large phantoms. Data from all tube potentials are pooled within each scanner group. Dashed line represents identity line.

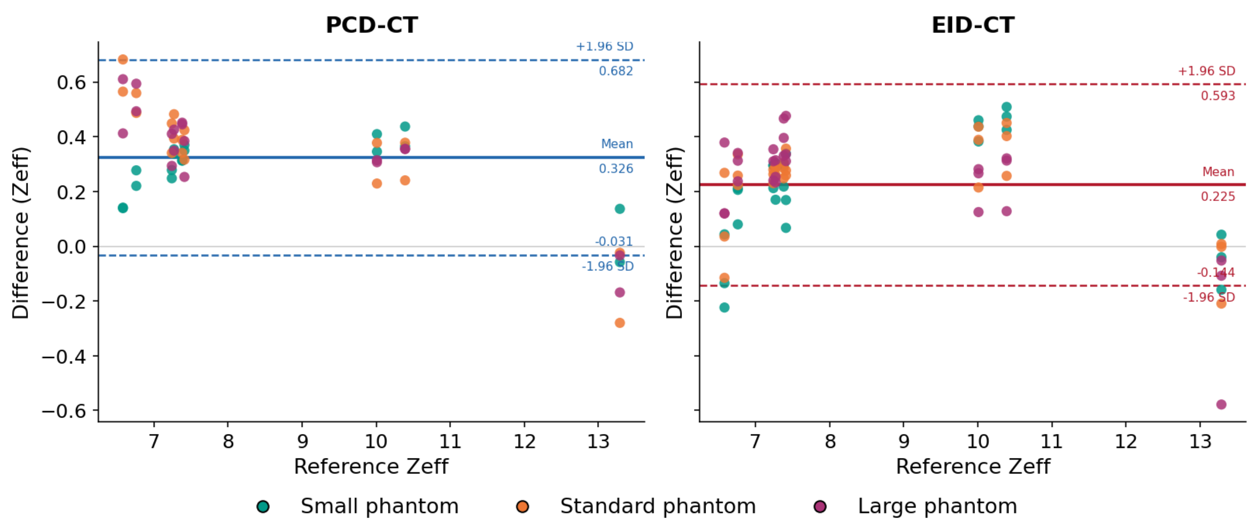

Figure 5. Bland-Altman plots for Z_{eff}, show the difference between measured and reference Z_{eff} plotted against reference Z_{eff} from PCD-CT (left) and EID-CT (right). All tube potentials pooled within each scanner.

Noise of RED Map

PCD-CT consistently showed lower noise compared with EID-CT:

- PCD-CT: 0.008–0.013 vs. EID-CT: 0.012–0.021

An approximate 25–50% noise reduction across phantom sizes.

DISCUSSION

- PCD-CT improves quantitative stability of electron density, particularly at higher tube potentials, likely due to improved photon statistics and reduced electronic noise and cross scatter.
- RED noise was lower with PCD-CT compared to EID-CT across all phantom sizes, including the large phantom which represents a challenging imaging condition due to higher beam attenuation and increased photon starvation.
- Z_{eff} estimation remained stable across systems, indicating that current decomposition algorithms, rather than detector technology, may be the limiting factor for Z_{eff} accuracy.

CONCLUSIONS

- PCD-CT enhances electron density quantification by improving accuracy and reducing noise, particularly in larger body simulations and at higher tube potentials.
- Z_{eff} estimation remains consistent across PCD-CT and EID-CT, with minimal dependence on scan conditions.
- Overall, PCD-CT provides improved performance for quantitative CT imaging, supporting its potential role in radiotherapy planning and material characterization.

ACKNOWLEDGEMENTS

Research reported in this work was supported in part by the NIH under award number R01 EB038746 and the Mayo Clinic Graduate School of Biomedical Sciences.

REFERENCES

1. Hu G, Niepel K, Risch F, et al. Assessment of quantitative information for radiation therapy at a first-generation clinical photon-counting computed tomography scanner. Front Oncol. 2022;12:970299. Published 2022 Sep 14. doi:10.3389/fonc.2022.970299
2. Paganetti H. Range uncertainties in proton therapy and the role of Monte Carlo simulations. Phys Med Biol. 2012;57(11):R99-R117. doi:10.1088/0031-9155/57/11/R99
3. McCollough CH, Leng S, Yu L, Fletcher JG. Dual- and Multi-Energy CT: Principles, Technical Approaches, and Clinical Applications. Radiology. 2015;276(3):637-653. doi:10.1148/radiol.2015142631
4. Landry G, Seco J, Gaudreault M, Verhaegen F. Deriving effective atomic numbers from DECT based on a parameterization of the ratio of high and low linear attenuation coefficients. Phys Med Biol. 2013;58(19):6851-6866. doi:10.1088/0031-9155/58/19/6851
5. Leng S, Bruesewitz M, Tao S, et al. Photon-counting Detector CT: System Design and Clinical Applications of an Emerging Technology. Radiographics. 2019;39(3):729-743. doi:10.1148/rg.2019180115
6. Rajendran K, Petersilka M, Henning A, et al. First Clinical Photon-counting Detector CT System: Technical Evaluation. Radiology. 2022;303(1):130-138. doi:10.1148/radiol.212579

Contact information: sadeghiansharafi.maryam@mayo.edu